Journal of Applied Physics

RESEARCH ARTICLE | JUNE 02 2022

Challenges in double-beam laser interferometry measurements of fully released piezoelectric films

Tianning Liu ; Pannawit Tipsawat ; Wanlin Zhu ; Thomas N. Jackson ; Mani Sivaramakrishnan ; Peter Mardilovich ; Thorsten Schmitz-Kempen ; Susan Trolier-McKinstry

J. Appl. Phys. 131, 214102 (2022)
https://doi.org/10.1063/5.0090278
CHORUS

AIP Publishing

Journal of Applied Physics ARTICLE scitation.org/journal/jap

Challenges in double-beam laser interferometry measurements of fully released piezoelectric films

Cite as: J. Appl. Phys. **131**, 214102 (2022); doi: 10.1063/5.0090278
Submitted: 4 March 2022 · Accepted: 6 May 2022 ·
Published Online: 2 June 2022

Tianning Liu,[1] Pannawit Tipsawat,[1] Wanlin Zhu,[2] Thomas N. Jackson,[1,2] Mani Sivaramakrishnan,[3] Peter Mardilovich,[4,a)] Thorsten Schmitz-Kempen,[4] and Susan Trolier-McKinstry[1,2]

AFFILIATIONS

[1]School of Electrical Engineering and Computer Science, Pennsylvania State University, University Park, Pennsylvania 16802, USA
[2]Department of Materials Science and Engineering, Pennsylvania State University, University Park, Pennsylvania 16802, USA
[3]ARNDIT LLC, Beaverton, Oregon 97007, USA
[4]AixACCT Systems GmbH, Aachen 52068, Germany

[a)]**Author to whom correspondence should be addressed:** mardilovich@aixacct.com

ABSTRACT

When utilizing double-beam laser interferometry to assess the piezoelectric coefficient of a film on a substrate, probing both top and bottom sample surfaces is expected to correct the erroneous bending contribution by canceling the additional path length from the sample height change. However, when the bending deformation becomes extensive and uncontrolled, as in the case of membranes or fully released piezoelectric films, the double-beam setup can no longer account for the artifacts, thus resulting in inflated film displacement data and implausibly large piezoelectric coefficient values. This work serves to identify these challenges by demonstrating $d_{33,f}$ measurements of fully released PZT films using a commercial double-beam laser interferometer. For a 1 μm thick randomly oriented PZT film on a 10 μm thick polyimide substrate, a large apparent $d_{33,f}$ of 9500 pm/V was measured. The source of error was presumably a distorted interference pattern due to the erroneous phase shift of the measurement laser beam caused by extensive deformation of the released sample structure. This effect has unfortunately been mistaken as enhanced piezoelectric responses by some reports in the literature. Finite element models demonstrate that bending, laser beam alignment, and the offset between the support structure and the electrode under test have a strong influence on the apparent film $d_{33,f}$.

INTRODUCTION

Understanding the electrical and piezoelectric responses in fully released piezoelectric films is important for the development of flexible piezoelectric-micro-electromechanical-system (piezoMEMS). For piezoelectric films grown on rigid substrates, substrate-clamping lowers piezoelectric and dielectric responses relative to those seen in bulk counterparts, due to a restricted in-plane deformation and reduced non-180° domain wall motion.[1–3] Lefki and Dormans developed a model relating the effective longitudinal piezoelectric coefficient for films, $d_{33,f}$, for films on a rigid substrate, to the coefficients d_{33} and d_{31} of the same bulk material, as[4]

$$d_{33,f} = d_{33} - 2d_{31}\frac{s_{13}^E}{(s_{11}^E + s_{12}^E)}, \quad (1)$$

where s_{11}, s_{12}, and s_{13} are the elastic compliance coefficients of the film. In Eq. (1), d_{31} and s_{13} are negative, $|d_{31}|$ is about one half of d_{33} and $|s_{13}/(s_{11}+s_{12})| < 1$, and hence it follows that the effective longitudinal piezoelectric coefficient ($d_{33,f}$) for films is smaller, by default.

Many reports have demonstrated improved domain reorientation and enhanced piezoelectric responses via laterally patterning the films or locally removing the underlying substrate.[3,4–8] A previous report demonstrated substantially enhanced electrical properties in PZT films in fully released piezoelectric films on transfer from Si to 5 μm thick polyimide substrates.[9] Based on these results, a significant increase in the piezoelectric response is also anticipated: $d_{33,f}$ should approach d_{33}, the value of a bulk ceramic due to the reduced in-plane clamping force. Despite the fact that the effective longitudinal piezoelectric coefficient for films, $d_{33,f}$, can approach the d_{33} value if the in-plane clamping forces are close to zero, in this paper we always denote the value of the effective longitudinal coefficient of thin films by $d_{33,f}$ for consistency.

Although a variety of techniques are available to accurately assess the piezoelectric responses of films on a rigid substrate, there are very few reports in the literature demonstrating how to best quantify the piezoelectric coefficient for films on flexible polymeric substrates. In fact, the techniques used for rigid substrate-based testing might not be readily implementable for flexible substrate-based films due to hidden pitfalls that could potentially result in inflated data and compromised accuracy. This work serves to identify these conditions by measuring $d_{33,f}$ of PZT thin-films on flexible polyimide substrates using a commercial double-beam laser interferometer (DBLI).

In a DBLI system, the laser source is divided into a reference beam and a measurement beam. The measurement beam is directed to both the top and the bottom sample surfaces before interfering with the reference laser beam to form an interference pattern, of which the intensity is measured by a photodetector. Any changes in the thickness of the sample will alter the path length of the measurement beam, thus changing the intensity contrast of the interference pattern. The sample displacement under an applied electric excitation is, therefore, quantified based on the intensity change. Probing both top and bottom surfaces accounts for bending that occurs in testing piezoelectric films on a rigid substrate;[10] this contribution is eliminated as the additional path lengths traveled by the two measurement beams cancel each other. Although bending of rigid substrate-based samples can be compensated by the DBLI approach, significant bending of a membrane structure or fully released flexible films on polymer substrates can introduce artifacts that are beyond the correctable limit of the DBLI instrument for typical silicon wafers and result in inflated measurement data.

SAMPLE FABRICATION

The fabrication of the fully released PZT films on polyimide substrates incorporated the release-and-transfer technique demonstrated in a previous report.[9] A 100 nm thick ZnO release layer and a 10 nm thick Al_2O_3 diffusion barrier layer were deposited on a clean 100 mm Si wafer with a 1 μm thick thermal oxide layer. This was done in a custom-built plasma enhanced atomic layer deposition (PEALD) system at 200 °C. The metalorganic precursors used for growing the oxide layers were DEZ and TMA for ZnO and Al_2O_3, respectively; the oxidant gases were N_2O for ZnO and CO_2 for Al_2O_3. Next, a 100 nm thick Pt was deposited on the Al_2O_3 at room temperature in a Kurt J. Lesker CMS 18 DC magnetron sputtering system (Pittsburgh, PA, USA) and patterned lithographically by lift-off to form the first electrode layer (top electrode upon release). This layer adopted the pattern shown schematically in Fig. 1(a), consisting of circles 800 μm in diameter and extension tabs for flexible cable connections.

Next, a 1 μm thick $Pb(Zr_{0.52},Ti_{0.48})O_3$ layer with 2% Nb doping was deposited over the patterned platinum electrodes via chemical solution deposition by spin-coating Mitsubishi E1 solution (Mitsubishi Materials, Tokyo, Japan). The films were crystallized in an AccuThermo AW 810 rapid thermal annealing (RTA) system at 700 °C for 1 min in air. These steps were repeated 12 times to reach a desired thickness of ~1 μm. A 0.08 M PbO capping layer was applied after 12 layers of PZT coating to convert any surface pyrochlore on the PZT to perovskite. A 100 nm thick blanket Pt layer was sputter-deposited on the PZT at room temperature to serve as the second electrode layer (bottom electrode upon release).

Before introducing the flexible transfer substrate, a 30 nm thick Al_2O_3 barrier layer was deposited on the blanket Pt bottom electrode by PEALD to prevent PZT degradation resulting from poly(amic acid) imidization.[11] Then, PI-2611 poly(amic acid) precursor solution was spin-coated on the Al_2O_3-protected Pt and imidized in a tube furnace at 305 °C in Ar for 75 min. The thickness of the polyimide layer was 10 μm.

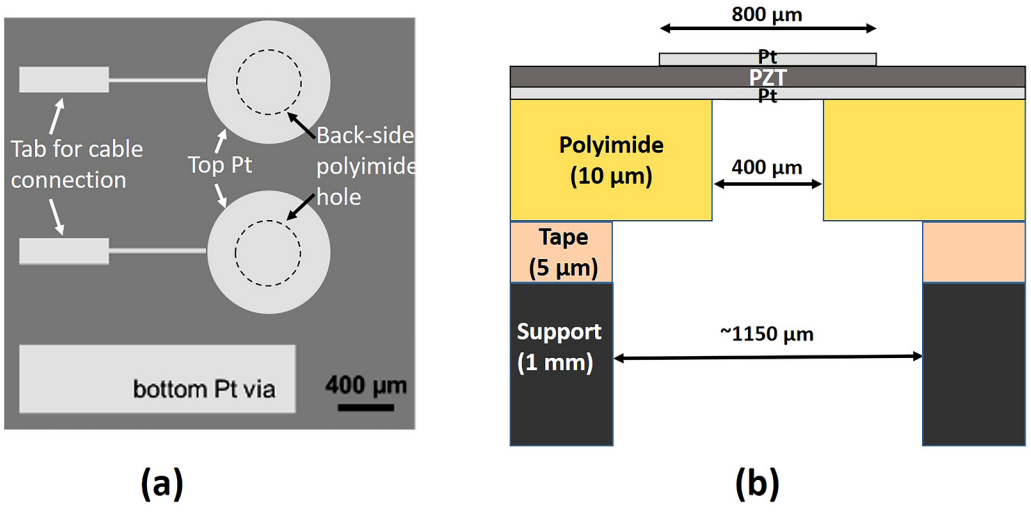

FIG. 1. Schematic configuration of the fully released PZT films. (a) Top-down view of the top electrode pattern with respect to the polyimide cavity. (b) Cross section of the released sample on polycarbonate carrier. Both polyimide and carrier have openings to allow direct laser probing on the bottom Pt.

To allow direct laser probing on the bottom Pt, windows were etched in the polyimide layer through reactive ion etching in a PlasmaTherm 720 system (Fremont, CA, USA) in 100% O_2 at 100 mTorr and −200 V substrate DC bias. The windows were 400 μm circles concentric with the top Pt circles, as shown in Fig. 1. A 50 nm thick Al layer was used as the hard etch-mask, as the etch rate of Al in fluorine plasma is negligible due to the low vapor pressure of AlF_3.[12] The Al layer was deposited in an RF magnetron sputtering system (Kurt J. Lesker CMS-18) and patterned by wet-etching in 0.26*N* tetramethylammonium hydroxide (TMAH). After polyimide patterning, the Al etch mask was removed in a 0.26*N* TMAH bath for 2 min. The sample was then rinsed with DI water and dried with clean compressed air before being transferred to a 50 °C, 50% acetic acid bath to dissolve ZnO and facilitate release.

To accommodate the frame-type vacuum chuck on the DBLI system, the fully released flexible sample was attached onto a 1 mm thick polycarbonate carrier. This provided mechanical support and allowed the sample to remain approximately flat during testing. The carrier piece had a small trench-shaped opening to expose the bottom electrode, as shown schematically in Fig. 1(b). The sample was adhered to the carrier using a thin double-sided tape with a matching opening as the carrier. To form electrical connections, a flexible ribbon cable was attached to the electrode tabs with anisotropic conductive films (ACFs).[13,14] The other end of the flexible cable was ACF-bonded to a printed circuit board connected with pin-headers accessing each electrode. (The use of needle probes should be avoided here as they deform the samples, deflecting the laser beam and inducing loss of the optical signal. Additionally, the physical contact between the probe and the flexible sample was unreliable, resulting in loss of the electrical signal as soon as the sample began to actuate.) Figure 2(a) shows the sample setup after being loaded on the DBLI system.

DBLI MEASUREMENT

An aixACCT DBLI system (Aachen, Germany) equipped with a 632.8 nm He-Ne laser with ∼1 pm vertical resolution was used to assess the $d_{33,f}$. The PZT was poled at 13 V (3× coercive field) at room temperature for 20 min. The sample was loaded on the DBLI system with the polycarbonate carrier vacuum-held by the frame-chuck. The center of the top electrode was aligned to the top laser beam by eye through the microscope, assuming a centering accuracy of less than 100 μm. The bottom laser beam was vertically aligned to the top beam as a default setting of the instrument. Figure 2(b) shows the camera view of the testing electrode with the top laser beam activated.

The testing electrodes were driven with two types of electrical excitation: (1) a large AC signal with zero DC bias and (2) a small AC signal with large DC bias. The denotation "large" is for electric fields with the amplitude comparable to, or larger than, the coercive field of the piezoelectric while the term "small" is for a fraction of the coercive field level.

For the large signal testing, the top electrode was excited by an 8 V triangular AC signal at 100 Hz. Polarization and displacement in the three directions are presented in Fig. 3(a) with respect to the amplitude of the excitation. While the polarization results are within the correct range, the detected displacement reached 50 nm, indicating a 5% strain level, which was five times larger than the reported strain limit for most PZT thin films. Based on the slope of the linearly fitted decreasing field displacement curve, the $d_{33,f}$ was evaluated as 9500 pm/V, which was two orders of magnitude larger than similar PZT films on rigid substrates (110–140 pm/V),[6,15] and even extensively exceeds the d_{33} of bulk ceramic PZT5A (∼304 pm/V).[6] In terms of small signal measurements, the electrode was driven with a 0.05 V AC signal at 1 kHz superimposed on a DC bias voltage sweeping between 0 and 8 V. The small-signal results are shown in Fig. 3(b) as permittivity and $d_{33,f}$ plotted against the DC bias. While the permittivity values were verified with an LCR meter and showed consistent results, the $d_{33,f}$ oscillated between implausibly large 4000 and 7000 pm/V. These results strongly suggested that artifacts existed in the measurement regime, which were not being accounted for by the DBLI system; as the electrical properties were correct, the source of errors was presumably from the optical signal.

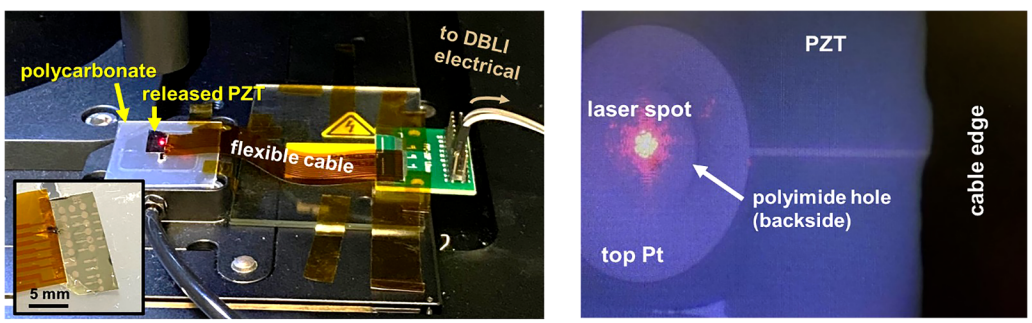

FIG. 2. Testing setup on the DBLI system. (a) Released PZT film on a polycarbonate backing and connected to a printed circuit board through ACF-bonding a piece of flexible ribbon cable. (b) The top surface of the testing sample viewed by the system's camera. The top laser incidence is centered on the top electrode circle. Judging by the faintly visible outline of the backside polyimide window, the bottom laser beam is expected to be directly probing the bottom Pt as the two beams are aligned by default.

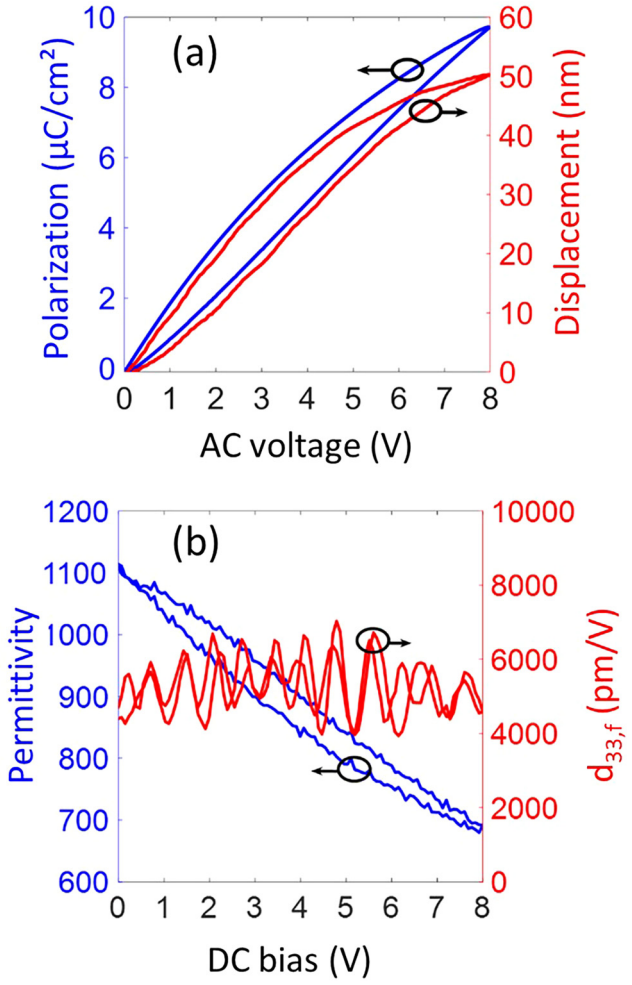

FIG. 3. (a) Large-signal measurement with 8 V AC excitation at 100 Hz. The slope of the displacement curve fitted linearly between 0 and 1 V gave a $d_{33,f}$ value of 9500 pm/V. (b) Small signal measurement with 0.05 V AC excitation at 1 kHz superimposed on a DC bias from 0 to 8 V. The measured $d_{33,f}$ values are on the same order of magnitude as (a).

To further examine the sample displacement behavior, single-beam laser interferometry measurement was conducted on the top sample surface. Using the single-beam function of the same instrument, a 5 V peak triangular AC signal was applied at 100 Hz to the same electrodes. The measured displacement along the thickness direction and the polarization are shown in Fig. 4 as a function of the AC voltage amplitude. The single-beam testing detected an even larger top surface displacement of 1.5 μm with the sign reversed from the double-beam experiments. The negative sign was an indication that bending was the dominating contribution in the detected out-of-plane response, as the transverse d_{31} coefficient bears the negative sign. The extremely large displacement presumably shifted the interferometry system out of the calibrated range for quantitative measurements. The interferometer range is also

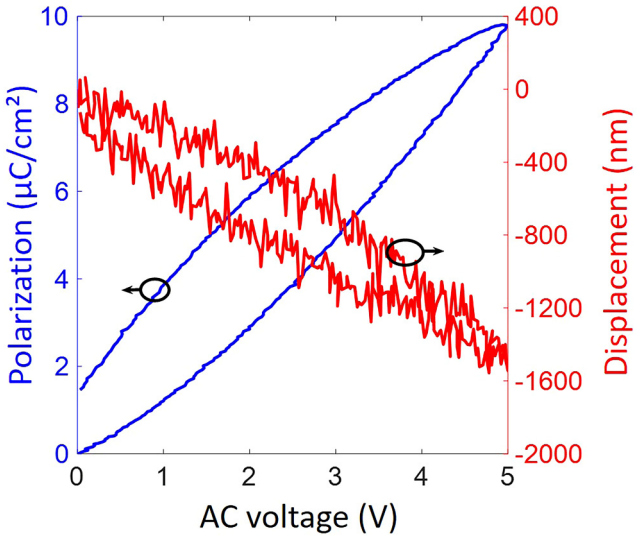

FIG. 4. The single-beam laser interferometry testing detected negative-signed, even larger displacement levels through probing the top Pt electrode driven between 0 and 5 V at 100 Hz. The data suggest that there is significant sample bending that is not being compensated by the interferometer system.

limited by the measurement principle[10] by the linear approximation of $\sin(4\pi\Delta L/\lambda) \approx 4\pi\Delta L/\lambda$ to an eighth of the laser wavelength of 632.8 nm, or further reduced to ~19 nm not to exceed a 1% error level. Exceeding this range will generate nonlinear artifacts.

Though the double-beam approach is expected to compensate the bending contribution, extensive bending in a released structure could potentially introduce additional distortion in the measurement laser beams. This is uncorrectable by the DBLI system. The beam deformation can be explained by the schematics in Fig. 5.

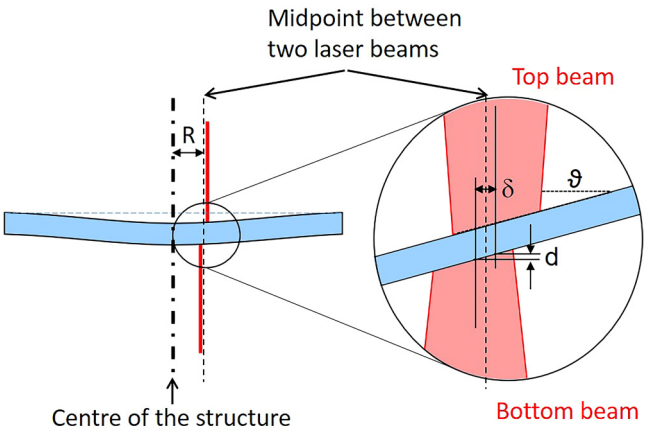

FIG. 5. Within the laser incidence, the sample tilt (θ) causes a parasitic displacement (*d*). *R* is the radial distance of the midpoint between the two laser beams from the center of the structure and δ is the beams misalignment (offset).

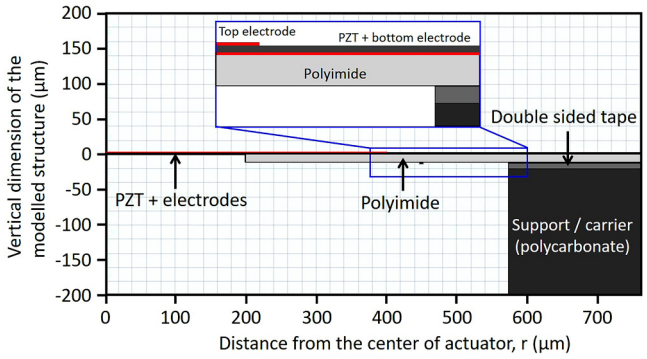

FIG. 6. Axi-symmetric geometry used in the finite element model. The inset shows the relative positions of the top electrode and the polycarbonate carrier.

The curvature of the sample generates a tilted mirror within the laser spot. Thus, the laser beam is not reflected perfectly perpendicular to the sample surface. Therefore, the focus is changed dynamically, influencing the size and position of the bottom reflection in addition to the alignment tolerance of the beams. Since the total membrane deflection within the laser spot area is several orders of magnitude higher than the actual thickness expansion, the bending contribution can no longer be completely compensated.

This optical error may have been the reason why large apparent $d_{33,f}$ values were measured on released thin film $(1-x)Pb(Mg_{1/3}Nb_{2/3})O_3$-$xPbTiO_3$ (PMN-PT) on blanket polydimethylsiloxane (PDMS) substrates using the DBLI approach.[16] After transferring PMN-PT films from Si to a PDMS layer while being supported by glass, the $d_{33,f}$ coefficient was reported to increase from ~11 to ~1000 pm/V at 100 kV/cm for a PMN-0.6PT film. While there is expected to be a finite improvement in the piezoelectric response on release, it is also possible that the effect is artificially inflated as a result of a combination of the laser beam being deflected due to the large PMN-PT deformation, coupled with changes in the optical path length in the PDMS.

For the PZT films in this work, the substantial bending is likely a result of asymmetry in the sample structure and the continuous PZT layer. As the polyimide underneath the top electrode was not fully removed on the backside (Fig. 1), the polymer annulus presumably served as a passive layer that shifted the neutral axis away from the PZT. This asymmetry, along with the flexible characteristic of the polyimide, resulted in bending of large magnitude. The continuous PZT layer further deteriorated the situation as the entire sample was likely actuated globally by the activated PZT area under the testing electrode. As a result, two modifications on the sample structure are proposed to reduce the excess bending. First, the etched window in the polyimide should be no smaller than the top electrode so that the activated structure does not bear any asymmetry. Second, patterning the PZT layer into islands should reduce the global actuation.

FINITE ELEMENT MODELS

Double beam laser interferometry, unlike single beam techniques, can, in principle, cancel the contribution from structural bending to the measured value of $d_{33,f}$. However, when a large amount of bending occurs in thin flexible substrates, as in the present experiments, full correction is not possible. The situation is exacerbated by the practical limits to which the top and the bottom laser beams can be aligned; the larger the misalignment, the larger the errors in the apparent $d_{33,f}$. In this study, the offset between the beams is expected to be ~20 μm.

In order to develop a quantitative understanding of the bending contribution to the measured value of $d_{33,f}$ by DBLI, a finite element structural model was developed using COMSOL. Figure 6 shows a simple 2D axisymmetric geometry of the modeled structure. The layer structure of the stack and the material properties used in the simulation are listed in Table I. The effects of stress stiffening on bending were investigated using the geometric nonlinearity feature in COMSOL, which accounts for structural deformation in the calculation of strain.

The modeling showed that the extent of bending and its contribution to the measured $d_{33,f}$ is very strongly dependent on the relative position of the punched hole in the carrier with respect to the edge of the top electrode, as illustrated by the inset in Fig. 6. Simulations were performed for various values of the punched hole diameter. For quantitative extraction from the model, $d_{33,f,model}$ is defined as the vertical displacement (w) of the point where the top laser beam hits the surface of the structure relative to the point where the bottom laser beam hits the surface,

$$d_{33,f,model} = w(top) - w(bottom). \quad (2)$$

Furthermore, there are two possible configurations of the offset between the two laser beams. In the first configuration (A), the top beam is located at $(R + \delta/2)$ while the bottom laser is located at $(R - \delta/2)$, where R is the radial distance of the midpoint between the two laser beams from the center of the structure and δ

TABLE I. Layers, materials, and the material properties of the stack structure.

Layer	Material	Thickness (μm)	Modulus (GPa)	Poisson's ratio	Density (kg/m^3)
Top electrode	Pt	0.1	168	0.38	21 450
PZT	PZT	1	65	0.38	7750
Bottom electrode	Pt	0.1	168	0.38	21 450
Flexible substrate	Polyimide	10	10	0.3	1500
Double-sided tape	Nitto No. 5600	5	2	0.3	5600
Carrier	Polycarbonate	1000	2.3	0.36	5600

is the offset between the two laser beams, as shown in Fig. 5. In configuration (B), the top beam is located at $(R-\delta/2)$ and the bottom beam is located at $(R+\delta/2)$. These two configurations occur in the measurement as the laser beams are scanned across the device from one side of the center to the other. Since the precise location of the average beam positions is not known experimentally, the values of $d_{33,f,model}$ for both configurations were evaluated for various values of R.

Figure 7 shows the bending profiles at an actuation voltage of 1 V for various values of the punched hole radius in the carrier, with and without stress stiffening effects. It is seen that the normal bending of the structure downwards occurs only when the punched hole is outside the edge of the top electrode. As the hole moves under the top electrode, the bending profiles become complicated. When the edge of the hole lies under the top electrode, it is

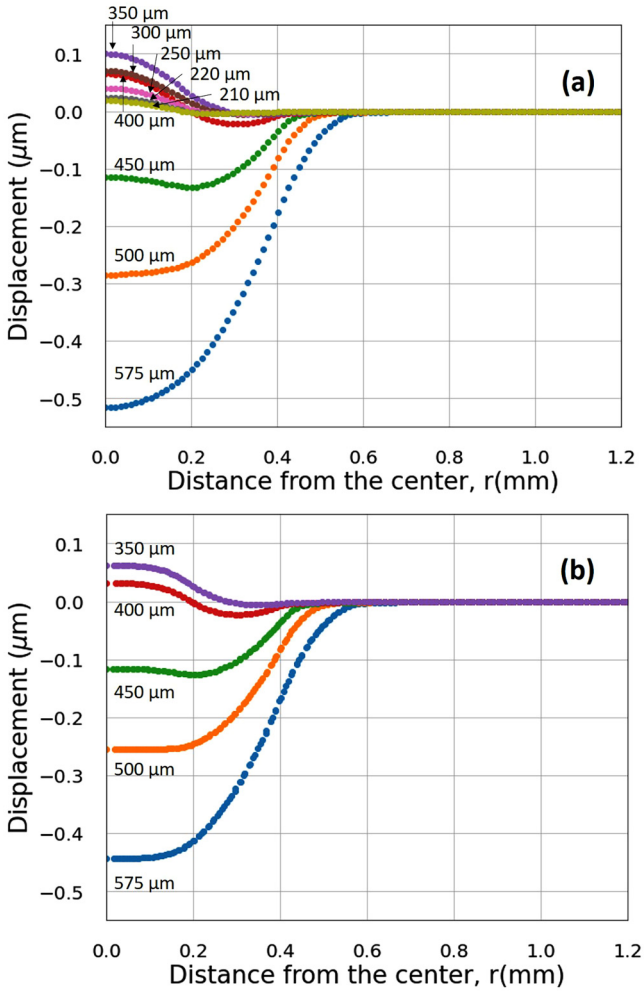

FIG. 7. Bending profiles for different punched hole diameter in the polycarbonate carrier (a) without stress stiffening and (b) with stress stiffening.

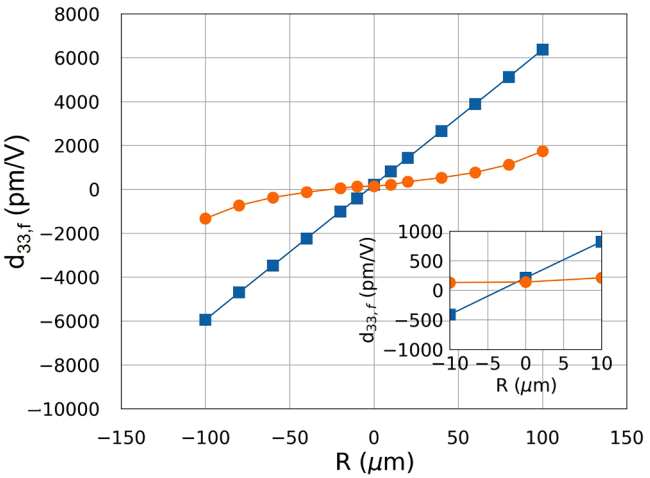

FIG. 8. d_33_f as extracted from the finite element model as the laser beams are scanned across the device: without stress stiffening (blue) and with stress stiffening (green). *R* is the radial distance of the midpoint between the two laser beams from the center of the structure.

believed that the complicated bending profiles are caused by the finite compliance of the carrier. If the structure could be rigidly attached to the carrier, then the bending profiles look normal for all values of the punched hole diameter (as shown in the supplement). It is also seen that stress stiffening not only reduces the magnitude of bending, but also affects the shape of the bending profiles, which, in turn, drastically reduces the apparent values of $d_{33,f}$. In order to highlight the bending contribution to the apparent $d_{33,f}$, the diameter of the punched hole was chosen to be 1.15 mm. $d_{33,f,model}$ vs R is plotted for both beam offset configurations, with and without stress stiffening effects in Fig. 8. It is clear that anomalously large values of $d_{33,f}$ are obtained from measurements when the bending is large. Furthermore, from the definition of $d_{33,f,model}$ in (2), it is evident that the bending contribution is positive for the first offset configuration (A: top beam at $R+\delta/2$) and negative for the alternate configuration (B: top beam at $R-\delta/2$), as shown in Fig. 8. As expected, the plots for the two offset configurations converge to the true value of $d_{33,f}$ when R = 0 with no offset between the two beams. The magnitude of $d_{33,f}$ increases linearly as the mean beam position moves radially out when the stress stiffening effects are not included, implying a parabolic bending profile. However, when the stress stiffening effects are included, $d_{33,f}$ vs beam position is nonlinear, implying a more complicated bending profile.

CONCLUSIONS

Challenges in DBLI measurements of unclamped longitudinal piezoelectric coefficient in fully released piezoelectric films were examined through testing 1 μm thick randomly oriented Pb$(Zr_{0.52}Ti_{0.48})_{0.98}Nb_{0.02}O_3$ films on 10 μm thick polyimide substrates using an aixACCT system. The test electrodes were circles of 800 μm in diameter on a blanket PZT film. Concentric circles of

400 μm in diameter were etched in polyimide to allow direct laser probing on the bottom Pt electrode. Measurements were conducted with large and small signal excitation, both of which measured d_{33} an order of magnitude larger than the maximum physically plausible value. The error source was suspected to be the phase shift in the laser beams as a result of significant bending in the sample system, which was presumably caused by the asymmetry in the structure as an annulus of the polyimide remained on the backside within the top electrode coverage. The continuous PZT configuration probably also encouraged the large-magnitude bending. The DBLI, in general, is suitable for testing piezoelectric thin films on substrates at typical wafer thicknesses as demonstrated from 200 up to 725 μm to receive reliable measurements.[17] However, it should be noted that the approaches described in Ref. 17 allow correction in the case of stiff inorganic substrates where the bending is moderate (e.g., for Si substrates with thickness exceeding 200 μm). This paper addresses the same issues in the case of flexible substrates where the bending is much more severe. It may also be noted that the main correction in the case of stiff substrates is the thickness increase due to the substrate stresses whereas much larger corrections are introduced due to the geometrical errors arising from severe bending in the case of flexible substrates. This is a very significant outcome of this study. Finally, while this paper addresses the challenges involved in the DBLI measurement of $d_{33,f}$ of films on flexible substrates by DBLI, our ultimate goal is to measure the true piezoelectric coefficients of such films, which are needed for the finite element modeling of the device performance. At present, a full set of data for released films with a wide range of flexible substrate thickness and different mechanical properties needed for such a goal is not available. This study, at best, is the first attempt to provide some of that data.

ACKNOWLEDGMENTS

This work was supported by: National Science Foundation (NSF) under Grant No. IIP-1547877 as part of I/UCRC Clusters for Grand Challenges: Center for Tire Research; NSF DMR–2025439 and MTEC Global Co., Ltd.

AUTHOR DECLARATIONS

Conflict of Interest

The authors have no conflicts to disclose.

DATA AVAILABILITY

The data that support the findings of this study are available from the corresponding author upon reasonable request.

REFERENCES

[1]A. Kholkin, "Non-linear piezoelectric response in lead zirconate titanate (PZT) films," Ferroelectrics **238**, 235–243 (2000).
[2]N. Bassiri-Gharb, I. Fujii, E. Hong, and S. Trolier-McKinstry, "Domain wall contributions to the properties of piezoelectric thin films," J. Electroceram. **19**, 47–65 (2007).
[3]S. Buhlmann, B. Dwir, J. Baborowski, and P. Muralt, "Size effect in mesoscopic epitaxial ferroelectric structures: Increase of piezoelectric response with decreasing feature size," Appl. Phys. Lett. **80**, 3195–3197 (2002).
[4]K. Lefki and G. J. M. Dormans, "Measurement of piezoelectric coefficients of ferroelectric thin films," J. Appl. Phys. **76**, 1764–1767 (1994).
[5]V. Nagarajan, A. Stanishevsky, L. Chen, T. Zhao, B.-T. Liu, J. Melngailis, A. L. Roytburd, R. Ramesh, J. Finder, Z. Yu, R. Droopad, and K. Eisenbeiser, "Realizing intrinsic piezoresponse in epitaxial submicron lead zirconate titanate capacitors on Si," Appl. Phys. Lett. **81**, 4215–4217 (2002).
[6]S. Shetty, J. I. Yang, J. Stitt, and S. Trolier-McKinstry, "Quantitative and high spatial resolution d_{33} measurement of piezoelectric bulk and thin films," J. Appl. Phys. **118**, 174104 (2015).
[7]F. Griggio, S. Jesse, A. Kumar, O. Ovchinnikov, H. Kim, T. N. Jackson, D. Damjanovic, S. V. Kalinin, and S. Trolier-McKinstry, "Substrate clamping effects on irreversible domain wall dynamics in lead zirconate titanate thin films," Phys. Rev. Lett. **108**, 157604 (2012).
[8]M. Wallace, R. L. Johnson-Wilke, G. Esteves, C. M. Fancher, R. H. T. Wilke, J. L. Jones, and S. Trolier-McKinstry, "*In situ* measurement of increased ferroelectric/ferroelastic domain wall motion in clamped tetragonal lead zirconate titanate thin films," J. Appl. Phys. **117**, 054103 (2015).
[9]T. Liu, M. Wallace, S. Trolier-McKinstry, and T. N. Jackson, "High temperature crystallized thin-film PZT on thin polyimide substrates," J. Appl. Phys. **122**, 164103 (2017).
[10]A. L. Kholkin, C. Wutchrich, D. V. Taylor, and N. Setter, "Interferometric measurements of electric field-induced displacements in piezoelectric thin films," Rev. Sci. Instrum. **67**, 1935–1941 (1996).
[11]T. Liu, A. Dangi, J. N. Kim, S.-R. Kothapalli, K. Choi, S. Trolier-McKinstry, and T. Jackson, "Flexible thin-film PZT ultrasonic transducers on polyimide substrates," Sensors **21**, 1014 (2021).
[12]D. W. Hess, "Plasma etch chemistry of aluminum and aluminum alloy films," Plasma Chem. Plasma Process. **2**, 141–155 (1982).
[13]S.-M. Chang, J.-H. Jou, A. Hsieh, T.-H. Chen, C.-Y. Chang, Y.-H. Wang, and C.-M. Huang, "Characteristic study of anisotropic-conductive film for chip-on-film packaging," Microelectron. Reliab. **41**, 2001–2009 (2001).
[14]N. Takano, T. Fujinawa, and T. Kato, "Film technologies for semiconductor & electronic components," Hitachi Chemical Technical Report No. 55, 2013, pp. 20–23.
[15]V. Kovacova, N. Vaxelaire, G. Le Rhun, P. Gergaud, T. Schmitz-Kempen, and E. Defay, "Correlation between electric field induced phase transition and piezoelectricity in PZT films," Phys. Rev. B **90**, 140101R (2014).
[16]J. C. Frederick, "Structure-property relations in sputter deposited epitaxial (1-x)Pb($Mg_{1/3}Nb_{2/3}$)O_3-$x$$PbTiO_3$ thin films," Ph.D. dissertation (Department of Materials Science and Engineering, University of Wisconsin-Madison, 2017), pp. 94–117.
[17]S. Sivaramakrishnan, P. Mardilovich, A. Mason, A. Roelofs, T. Schmitz-Kempen, and S. Tiedke, "Electrode size dependence of piezoelectric response of lead zirconate titanate thin films measured by double beam laser interferometry," Appl. Phys. Lett. **103**, 132904 (2013).